The pH-dependent gating of the human voltage-gated proton channel from computational simulations

Christophe Jardin,*[a] Niklas Ohlwein, [a,b] Arne Franzen,[c] Gustavo Chaves,[a] and Boris Musset [a]

[a.] *Klinikum Nürnberg Medical School, Institute of Physiology, Pathophysiology and Biophysics, Nuremberg, Germany.*
[b.] *Klinik für Anästhesiologie und operative Intensivmedizin, Universitätklinik der Paracelsus Medizinischen Privatuniversität, Nuremberg, Germany.*
[c.] *Institute of Biological Information Processing, Molecular and Cellular Physiology (IBI-1), Forschungszentrum Jülich, Jülich, Germany*

Supplementary Information

System Preparation

A structural model of the transmembrane voltage-sensing domain (VSD) of the human voltage-gated channel H_V1 (hH_V1) was constructed via homology modeling to the crystal structure of the VSD of the *Ciona intestinalis* voltage-sensing phosphatase (*Ci*-VSP) in the resting state. Beside the structural peculiarities of the two experimental structures of H_V1 channels available to date (see "System preparation" of the main text for a detailed discussion), the choice of *Ci*-VSP was motivated by the conclusion by Li et al. that it represents a better template for hH_V1 than other channels[1]. We considered the amino acid sequence of the "minimal" hH_V1 channel that was identified by our group as the shortest fully functional hH_V1 channel. The modelled transmembrane domain starts at residue M91 (helix S1) and ends at residue S224 (helix S4), both located in the cytoplasm. The amino acid sequence of hH_V1 was retrieved from the UniprotKB/Swiss-Prot database[2] (Uniprot entry: Q96D96) and the crystal structure of *Ci*-VSP from the Protein Databank[3] (PDB ID: 4G80[4], chain T). We used the alignment of the hH_V1 and *Ci*-VSP amino acid sequences (residues 91-224 and 108-240 respectively) with T-COFFEE[5] of our previous work[6]. The similarity between the two sequences (VSD domain) is 46% which is good enough for the construction of a reliable structural model. Hundred structural models were generated with MODELLER9.18[7,8]. The five best models according to the Modeler objective function were structurally refined using the 3D Refine online server[9]. For each model submitted, five solutions were generated and ranked according to the 3Drefine and RWPlus scores. Finally, the model with the best 3DRefine and RWPlus scores was conserved for further works. Inspection with PROCHECK[10] revealed no structural problem. Our starting structure agrees with most of the structural features revealed by different studies. For example, a hydrophobic plug that separates the intra- and extracellular vestibules is formed by the four amino acid residues V109, F150, V177 and V178, as identified in [11]. The conserved selectivity filter, D112 in hH_V1, is correctly located directly above the HG[12]. The three S4 voltage-sensing arginines R1 to R3 are facing the channel pore, and the sidechains of R1 and R3 are accessible by the extra- and intracellular solvents respectively, as found e.g. in [13]. The sidechains of the two zinc cations binding histidine residues, H140 and H193, are properly exposed for binding the cations from the extracellular medium[14].

References:

1. Q. Li, R. Shen, J. S. Treger, S. S. Wanderling, W. Milewski, K. Siwowska, F. Bezanilla and E. Perozo, *Proceedings of the National Academy of Sciences of the United States of America*, 2015, **112**, E5926-5935.
2. UniProt Consortium, *Nucleic Acids Research*, 2019, **47**, D506–D515.
3. H. M. Berman, J. Westbrook, Z. Feng, G. Gilliland, T. N. Bhat, H. Weissig, I. N. Shindyalov and P. E. Bourne, *Nucleic Acids Research*, 2000, **28**, 235–242.

4. Q. Li, S. Wanderling, M. Paduch, D. Medovoy, A. Singharoy, R. McGreevy, C. A. Villalba-Galea, R. E. Hulse, B. Roux, K. Schulten, A. Kossiakoff and E. Perozo, *Nature Structural and Molecular Biology*, 2014, **21**, 244–252.
5. C. Notredame, D. G. Higgins and J. Heringa. *Journal of Molecular Biology*, 2000, **302**, 205–217.
6. C. Jardin, G. Chaves and B. Musset, *Biophysical journal*, 2020, **118**, 1221-1233.
7. B. Webb and A. Sali. *Current Protocols in Bioinformatics*, 2016, **54**, 5.6.1–5.6.37.
8. A. Sali and T. L. Blundell. *Journal of Molecular Biology*, 1993, **234**, 779–815.
9. D. Bhattacharya, J. Nowotny, R. Cao and J. Cheng. *Nucleic Acids Research*, 2016, **44**, W406–W409.
10. R. A. Laskowski, M. W. MacArthur, D. S. Moss and J. M. Thornton. 1993. PROCHECK: a program to check the stereochemical quality of protein structures. *Journal of Applied Crystallography*, 1993, **26**, 283–291.
11. R. Banh, V. V. Cherny, D. Morgan, B. Musset, S. Thomas, K. Kulleperuma, S. M. E. Smith, R. Pomès and T. E. DeCoursey, *Proceedings of the National Academy of Sciences of the United States of America*, 2019, **116**, 18951-18961.
12. B. Musset, S. M. Smith, S. Rajan, D. Morgan, V. V. Cherny and T. E. Decoursey, *Nature*, 2011, **480**, 273-277.
13. K. Kulleperuma, S. M. E. Smith, D. Morgan, B. Musset, J. Holyoake, N. Chakrabarti, V. V. Cherny, T. E. DeCoursey and R. Pomès, *Journal of General Physiology*, 2013, **141**, 445-465.
14. B. Musset, S. M. E. Smith, S. Rajan, V. V. Cherny, S. Sujai, D. Morgan and T. E. DeCoursey, *Journal of Physiology*, 2010, **588**, 1435-1449.

Table S1. Effects of the titratable and S4 arginine amino acids on H_V1 activity. n.a.: no data available.

Amino acid	Effect(s) on hH_V1
Lys 94	n.a.
His 99	H99A: slightly shifts Δ_{thr} to more positive[1]
Asp 112	D112A: fails to abrogate expression of voltage-dependent H^+ currents but causes positive shift in V_{thr} (for ΔpH=0)[1] D112 is THE proton selectivity filter[2] D112A/N/Q: decrease (small) currents[3] D112E: binding cooperativity abolished for GBTA but not for 2GBI[4] D160A/C/N (in *Ci*-H_V1): non-conducting channel[5,6,7] D160N (in *Ci*-H_V1): affects proton conduction; alterates opening; D160 is responsible for ΔpH-dependent gating[8] D160 (in *Ci*-H_V1): plays a role in Zn^{2+} binding[7] D66A/S/H (in NpH_V1): exhibit anion currents[9] D66E (in NpH_V1): proton selective (like WT)[9] D66C (in NpH_V1): non-conducting channel[9] D112N/H: decreases Zn^{2+} potency to modulate H_V1 gating[23]
Glu 119	E119A: small effect on H_V1 voltage dependence[1] E119A: does not affect binding cooperativity of both GBTA and 2GBI[4] E167 (in *Ci*-H_V1): participates to Zn^{2+} binding[7] E115 (in mH_V1): involved in Zn2+ binding[10] E119H: increases Zn^{2+} potency to modulate H_V1 gating[23] E119A: decreases Zn^{2+} potency to modulate H_V1 gating[23]
Asp 123	D123A: small effect on H_V1 voltage dependence[1] D123A: reduces binding cooperativity of GBTA[4] D123R: small increase of binding cooperativity for GBTA[4] D171 (in *Ci*-H_V1): does not participate to Zn^{2+} binding[7] D171A (in *Ci*-H_V1): shifts G(V) curve to more depolarized potentials; contributes to channel opening[11] D171E (in *Ci*-H_V1): proton current similar to WT[11] D119 (in mH_V1): involved in Zn2+ binding[10] D123H: increases Zn^{2+} potency to modulate H_V1 gating[23]
Lys 125	K125A: small effect on H_V1 voltage dependence[1] K125A: does not affect binding cooperativity of both GBTA and 2GBI[4]
Asp 130	D130A: slightly shifts Δ_{thr} to more positive[1] D130H: increases Zn^{2+} potency to modulate H_V1 gating[23]
Lys 131	K131A: shifts Δ_{thr} to more positive[1]
His 140	External Zn^{2+} binding site; Zn^{2+} competes with proton for binding at this site[1,2] H140A (with H193A simultaneously): similar pH-dependent gating as Wild Type[12] H188A (in *Ci*-H_V1): abolishes Zn2+ inhibition[7] H92A (in NpH_V1): participates in Zn^{2+} binding[13] H140A: decreases Zn^{2+} potency to modulate H_V1 gating[23]
Glu 153	E153A: fails to abrogate expression of voltage-dependent H^+ currents[1] E153N/A causes negative shift in V_{thr} (for ΔpH=0)[1] E153C: negative shift of voltage-dependent gating[14]

	E153A: decreases Zn^{2+} potency to modulate H_V1 gating[23]
Lys 157	K157A: fails to abrogate expression of voltage-dependent H^+ currents / negligible effect on H_V1 voltage dependence[1]
Glu 164	E164A (with E171A): slightly shifts Δ_{thr} to more negative[1]
His 167	H167A (with H168A simultaneously): similar pH-dependent gating as Wild Type[1] Not involved in internal pH sensing[15] H163S (in mH_V1): gating kinetics similar to WT[16]
His 168	H168A (with H167A simultaneously): similar pH-dependent gating as Wild Type[1] Internal pH sensor[15] H164S (in mH_V1): accelerates gating activation kinetics[16]
Lys 169	n.a.
Glu 171	E171A (with D174A): shifts Δ_{thr} to more positive[1] E171A: Normal initial H^+ flux followed by recovery ascribed to leak induced in vesicles[22]
Asp 174	D174A: fails to abrogate expression of voltage-dependent H^+ currents[1] D174N/A causes negative shift in V_{thr} (for ΔpH=0)[1]
Asp 185	D185A: fails to abrogate expression of voltage-dependent H^+ currents but causes positive shift in V_{thr} (for ΔpH=0)[1] Does not impair proton selectivity[2]
Glu 192	E192A (with E196A): slightly shifts Δ_{thr} to more positive[1]
His 193	External Zn^{2+} binding site; Zn^{2+} competes with proton to bind at this site[1,2] H193A (with H140A simultaneously): similar pH-dependent gating as Wild Type[12] E243W (in *Ci*-H_V1): slower deactivation kinetics[17] D145H (in NpH_V1): slows activation kinetics[13] D145A (in NpH_V1): does not participates in Zn^{2+} binding[13] H193A: decreases Zn^{2+} potency to modulate H_V1 gating[23]
Glu 196	E196A: decreases Zn^{2+} potency to modulate H_V1 gating[23]
Arg 205	R205A: faster activation and deactivation kinetics[12] R205H: similar to WT; accessible to external solvent in open state[18] R255N (in *Ci*-H_V1): decreases effective gating charge[19] R255A (in *Ci*-H_V1): restricts inward (but not outward) S4 movement[11] R205H: resting state H^+ shuttle current[20] R201Q (in mH_V1): faster activation kinetics[21]
Arg 208	R208A: faster activation and deactivation kinetics[12] R208H: similar to WT; accessible to external solvent in open state[18] R258N (in *Ci*-H_V1): decreases effective gating charge[19] R258C (in *Ci*-H_V1): accessible to internal solution in closed state but to external solution in open state[19]
Arg 211	R211A: faster deactivation kinetics[1] R211H: similar to WT; accessible to internal solvent in open state[18] R211S: binding cooperativity not affected for both GBTA and 2GBI[4] R261N (in *Ci*-H_V1): decreases effective gating charge[19] R207Q (in mH_V1): no change in activation kinetics[21] R163C (in NpH_V1): robust currents (smaller than WT)[9]
Lys 221	K221A: negligible effect on H_V1 voltage dependence[1] K221G: negligible effect on binding cooperativity of GBTA[4]

References:

1. I. S. Ramsey, Y. Mokrab, I. Carvacho, Z. A. Sands, M. S. P. Sansom and D. E. Clapham, *Nature Structural & Molecular Biology*, 2010, **17**, 869-875.
2. B. Musset, S. M. Smith, S. Rajan, D. Morgan, V. V. Cherny and T. E. Decoursey, *Nature*, 2011, **480**, 273-277.
3. Hong 2014: L. Hong, I. H. Kim and F. Tombola, *Proceedings of the National Academy of Sciences of the United States of America*, 2014, **111**, 9971-9976.
4. Hong 2015: L. Hong, V. Singh, H. Wulff and F. Tombola, *Scientific Reports*, 2015, **5**, 14077
5. Mony 2015: L. Mony, T. K. Berger, E. Y. Isacoff, *Nature Structural & Molecular Biology*, 2015, **22**, 283–290.
6. A. Chamberlin, F. Qiu, Y. Wang, S. Y. Noskov and H. Peter Larsson, *Journal of Molecular Biology*, 2015, **427**, 131-145.
7. Qiu 2016: F. Qiu, A. Chamberlin, B. M. Watkins, A. Ionescu, M. E. Perez, R. Barro-Soria, C. González, S. Y. Noskov and H. P. Larsson, *Proceedings of the National Academy of Sciences of the United States of America*, 2016, **113**, E5962-E5971.
8. Carmona 2021: E. M. Carmona, M. Fernandez, J. J. Alvear-Arias, A. Neely, H. P. Larsson, O. Alvarez, J. A. Garate, R. Latorre and C. Gonzalez, *Proceedings of the National Academy of Sciences of the United States of America*, 2021, **118**, e2025556118.
9. Chaves 2016: G. Chaves, C. Derst, A. Franzen, Y. Mashimo, R. Machida and B. Musset, *The FEBS Journal*, 2016, **283**, 1453-1464.
10. Okamura 2015: Y. Okamura, Y. Fujiwara and S. Sakata, *Annual Review of Biochemistry*, 2015, **84**, 685-709.
11. Qiu 2013: F. Qiu, S. Rebolledo, C. Gonzalez and H. P. Larsson, *Neuron*, 2013, **77**, 288-298.
12. Ramsey 2006: I. S. Ramsey, M. M. Moran, J. A. Chong and David E. Clapham, *Nature*, 2006, **440**, 1213-1216.
13. Chaves 2020: G. Chaves, S. Bungert-Plümke, A. Franzen, I. Mahorivska and B. Musset, *The FEBS Journal*, 2020, **287**, 4996-5018.
14. Tombola 2010: F. Tombola, M. H. Ulbrich, S. C. Kohout and E. Y. Isacoff, *Nature Structural & Molecular Biology*, 2010, **17**, 44-50.
15. Cherny 2018: V. V. Cherny, D. Morgan, S. Thomas, S. M. E. Smith and T. E. DeCoursey, *Journal of General Physiology*, 2018, **150**, 851-862.
16. S. Sakata, N. Miyawaki, T. J. McCormack, H. Arima, A. Kawanabe, N. Özkucur, T. Kurokawa, Y. Jinno, Y. Fujiwara and Y. Okamura, *Biochimica et Biophysica Acta*, 2016, **1858**, 2972-2983.
17. Okuda 2016: H. Okuda, Y. Yonezawa, Y. Takano, Y. Okamura and Y. Fujiwara, *Journal of Biological Chemistry*, 2016, **291**, 5931-5947.
18. Kulleperuma 2013: K. Kulleperuma, S. M. E. Smith, D. Morgan, B. Musset, J. Holyoake, N. Chakrabarti, V. V. Cherny, T. E. DeCoursey and R. Pomès, *Journal of General Physiology*, 2013, **141**, 445-465.
19. Gonzalez 2013: C. Gonzalez, S. Rebolledo, M. E. Perez and H. P. Larsson, *Journal of General Physiology*, 2013, **141**, 275-285.
20. Randolph 2016: A. L. Randolph, Y. Mokrab, A. L. Bennett, M. S. P. Sansom and I. S. Ramsey, *eLife*, 2016, **5**, e18017.
21. M. Sasaki, M. Takagi and Y. Okamura, *Science*, 2016, **312**, 589-592.
22. J. A. Letts, PhD Thesis, The Rockefeller University, New York.
23. V. De La Rosa, A. L. Benett and I. S. Ramsey, *Journal of General Physiology*, 2018, **150**, 863-881.

Supplementary figures

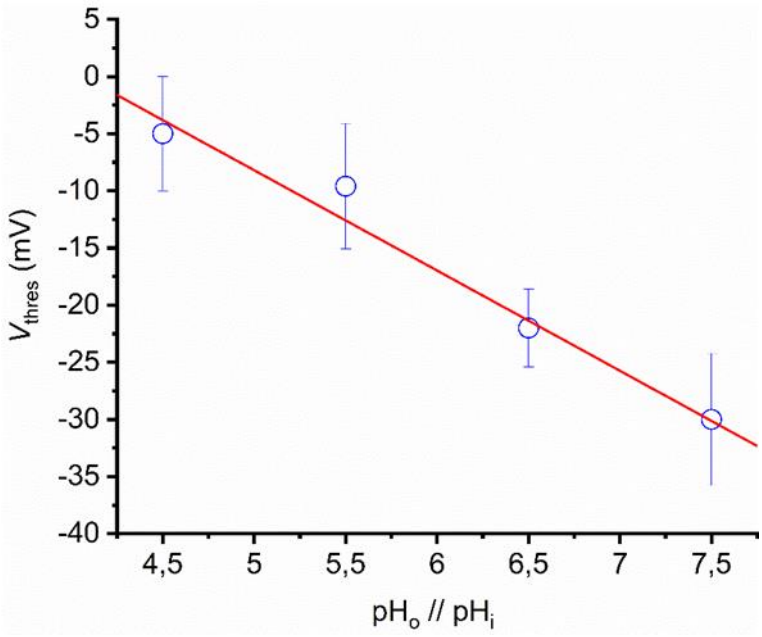

Fig. S1. Threshold of activation of hH_V1m at symmetrical pH is pH-dependent. The threshold of activation (V_{thres}) indicates the voltage at which the channel first opens during a family of depolarizing pulses. It is detected experimentally as the appearance of a characteristic H^+ tail current. The data is presented as Mean ± SEM at different symmetrical pH conditions (pH_o = extracellular, pH_i = intracellular). The red line represents a linear adjustment with an R^2 = 0,96055.

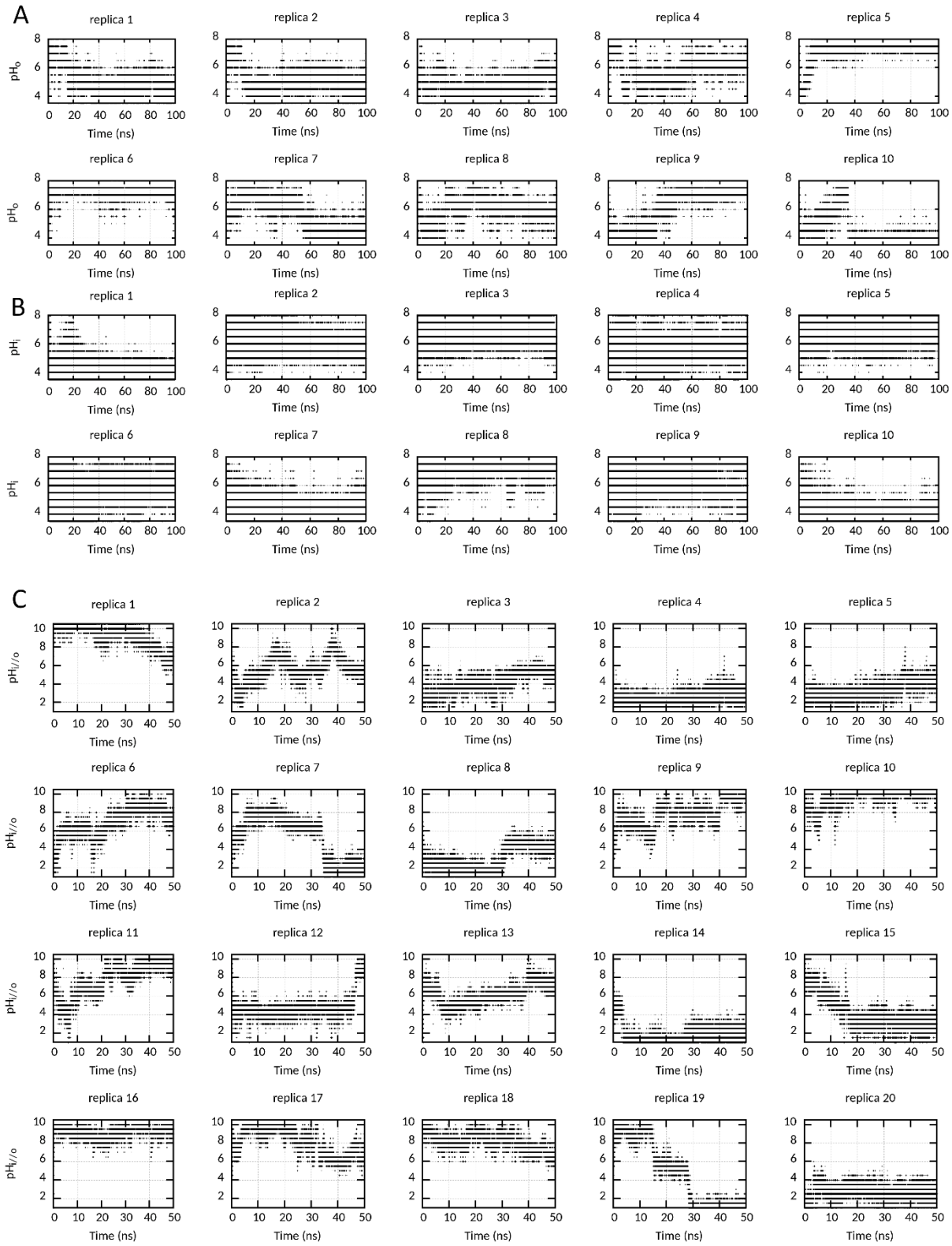

Figure S2. Replica walk in the pH-ladder during the (A) $\Delta pH_{i=cst}$, (B) $\Delta pH_{o=cst}$ and (C) pH_{sym} CpHRE MD simulations.

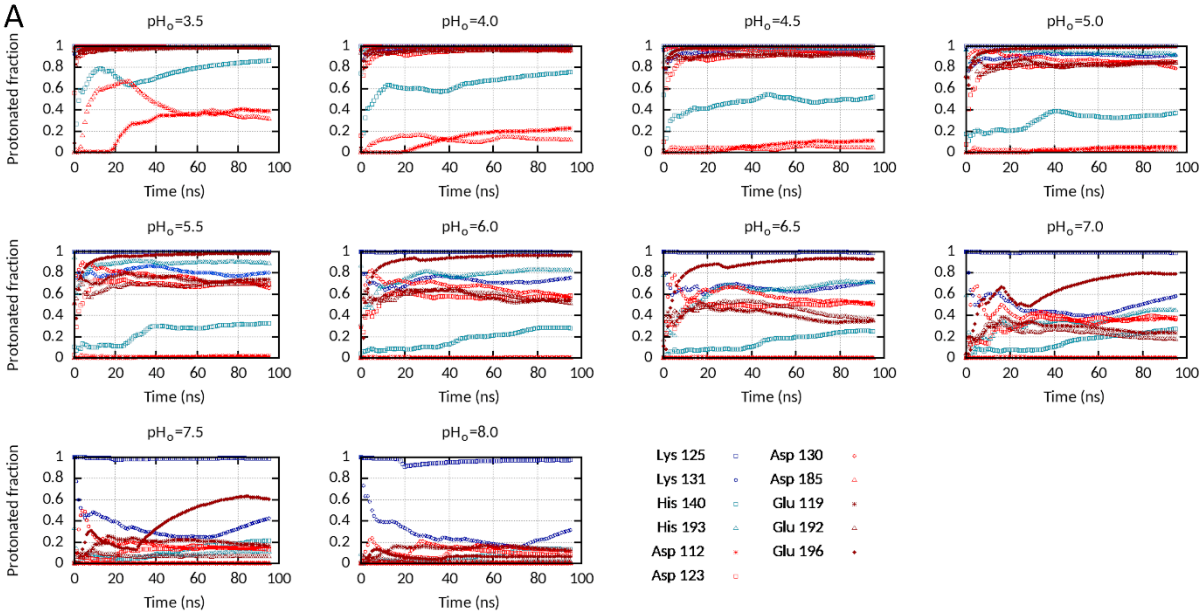
A
pH$_o$=3.5
pH$_o$=4.0
pH$_o$=4.5
pH$_o$=5.0
pH$_o$=5.5
pH$_o$=6.0
pH$_o$=6.5
pH$_o$=7.0
pH$_o$=7.5
pH$_o$=8.0
Protonated fraction
Time (ns)
Lys 125
Lys 131
His 140
His 193
Asp 112
Asp 123
Asp 130
Asp 185
Glu 119
Glu 192
Glu 196

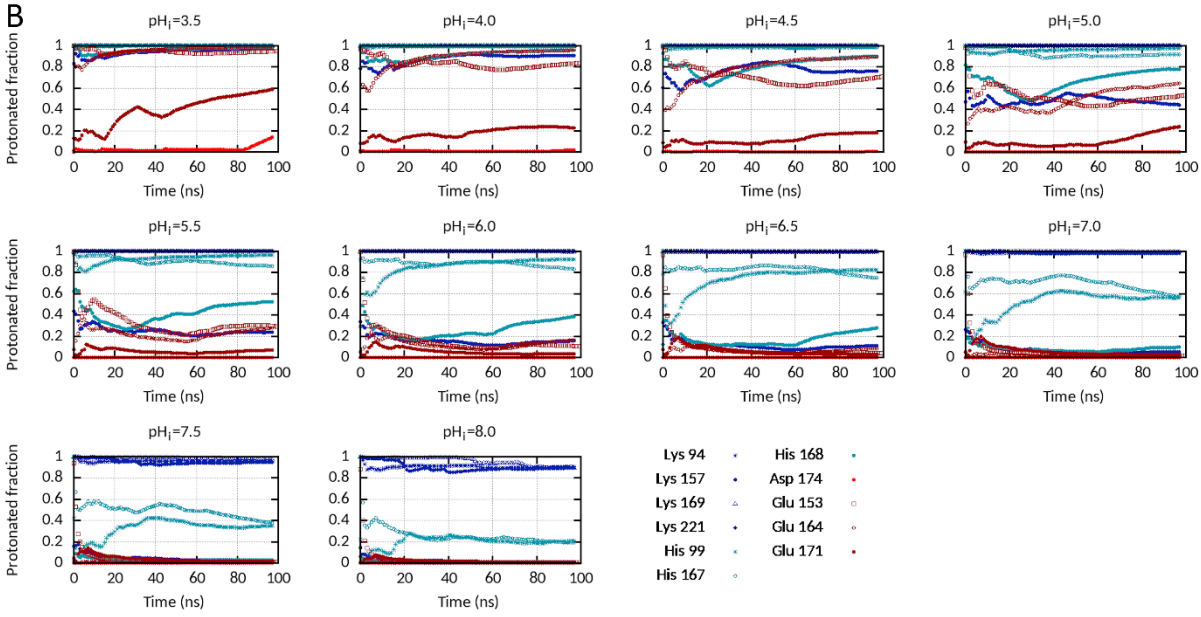
B
pH$_i$=3.5
pH$_i$=4.0
pH$_i$=4.5
pH$_i$=5.0
pH$_i$=5.5
pH$_i$=6.0
pH$_i$=6.5
pH$_i$=7.0
pH$_i$=7.5
pH$_i$=8.0
Protonated fraction
Time (ns)
Lys 94
Lys 157
Lys 169
Lys 221
His 99
His 167
His 168
Asp 174
Glu 153
Glu 164
Glu 171

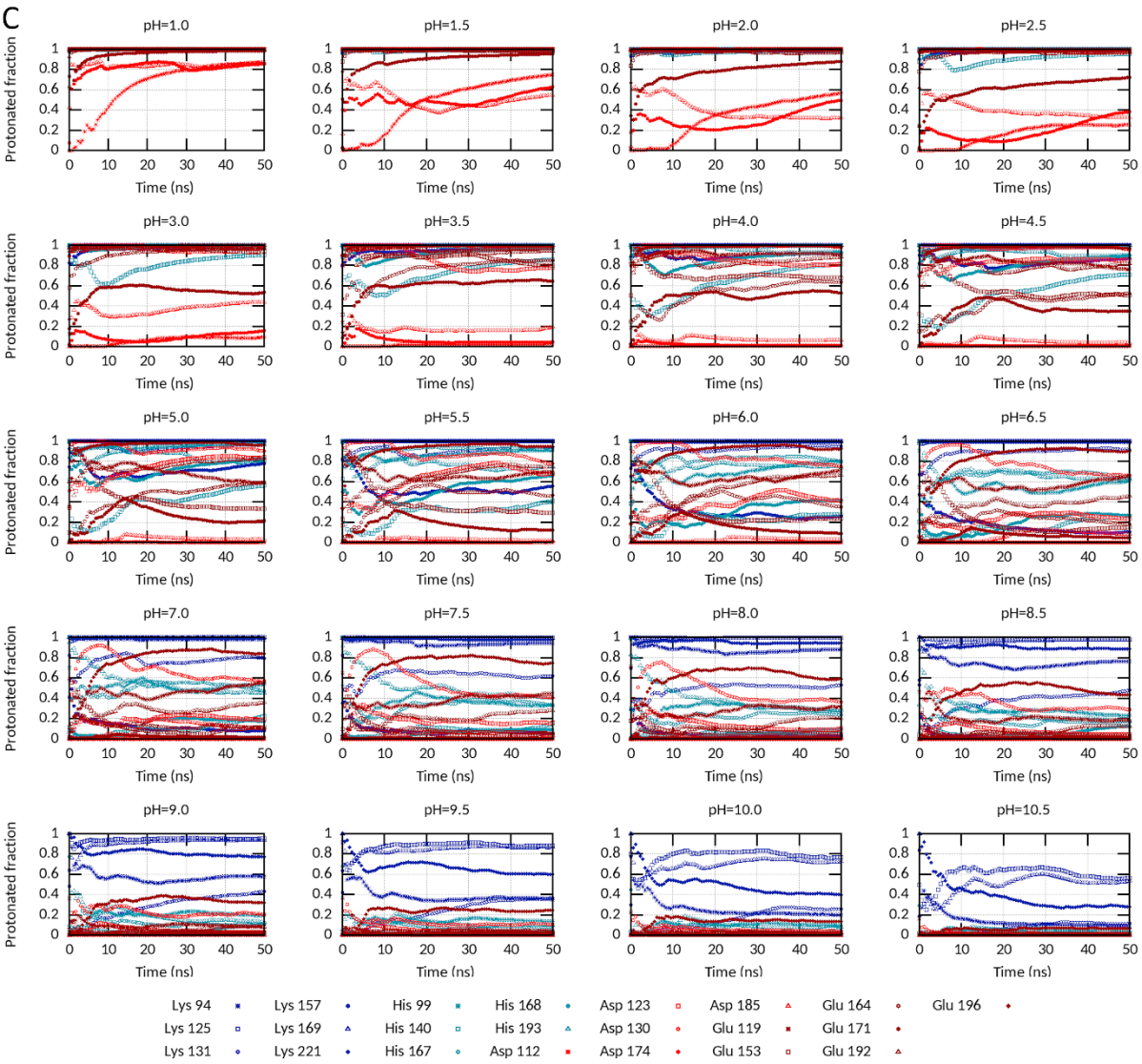

Figure S3. Cumulative protonated fraction during the (A) $\Delta pH_{i=cst}$, (B) $\Delta pH_{o=cst}$ and (C) pH_{sym} CpHRE MD simulations.

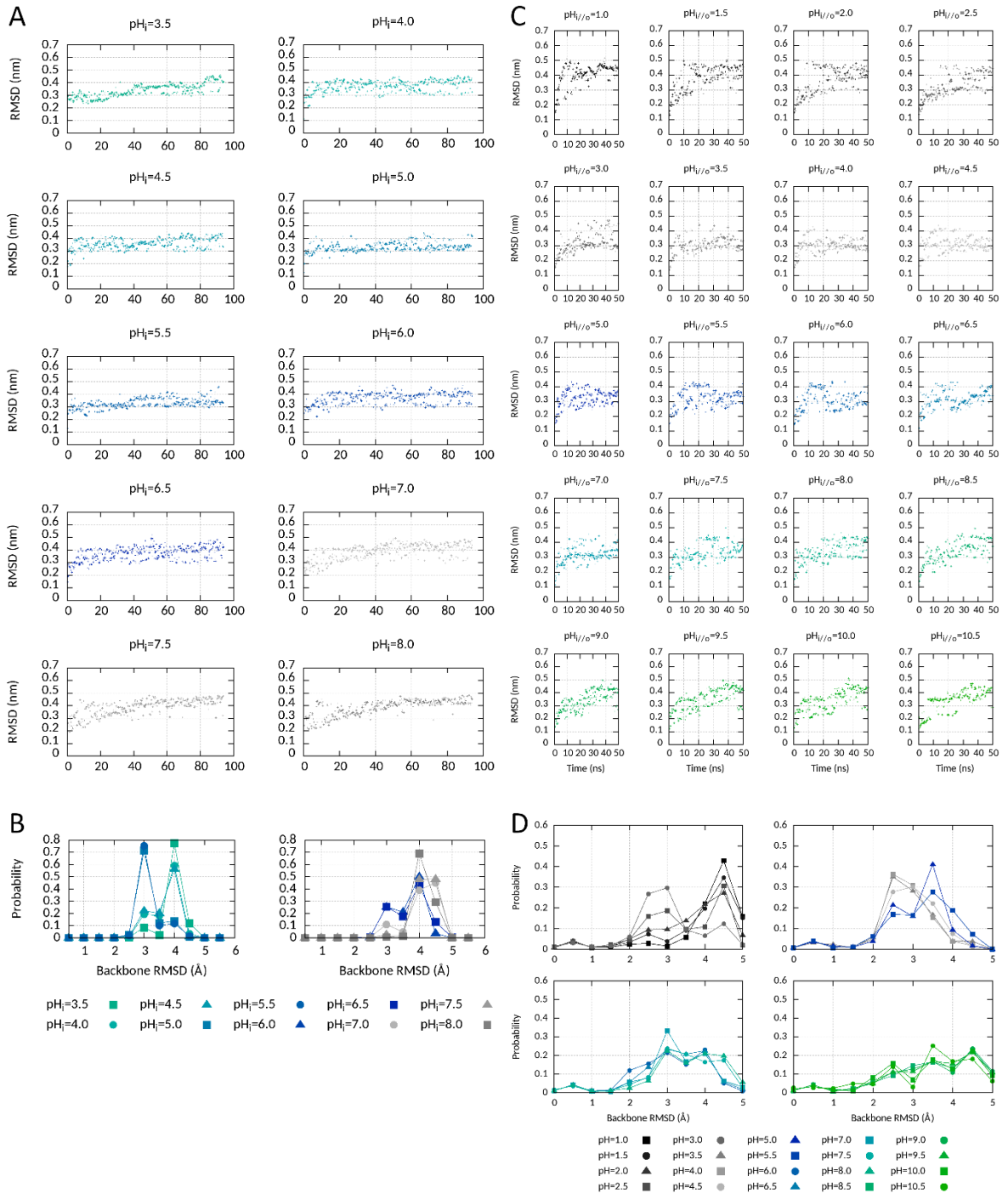

Fig. S4. Protein backbone RMSD at different pH_i values in the $\Delta pH_{o=cst}$ (A) and different symmetrical pH values in the pH_{sym} CpHRE MD simulations (C). Probability distribution of the protein backbone RMSD at different pH_i values in the last 10 ns of the $\Delta pH_{i=cst}$ CpHRE MD simulation (B) and at different symmetrical pH values in the last 10 ns of the pH_{sym} CpHRE MD simulation (D). In B) and D), the RMSD values were binned in bins with intervals of 0.5 Å. For example, a pic centered at 3.0 Å contains all the snapshots accumulated during the simulated time with 3.0 ≤ RMSD (Å) < 3.5.

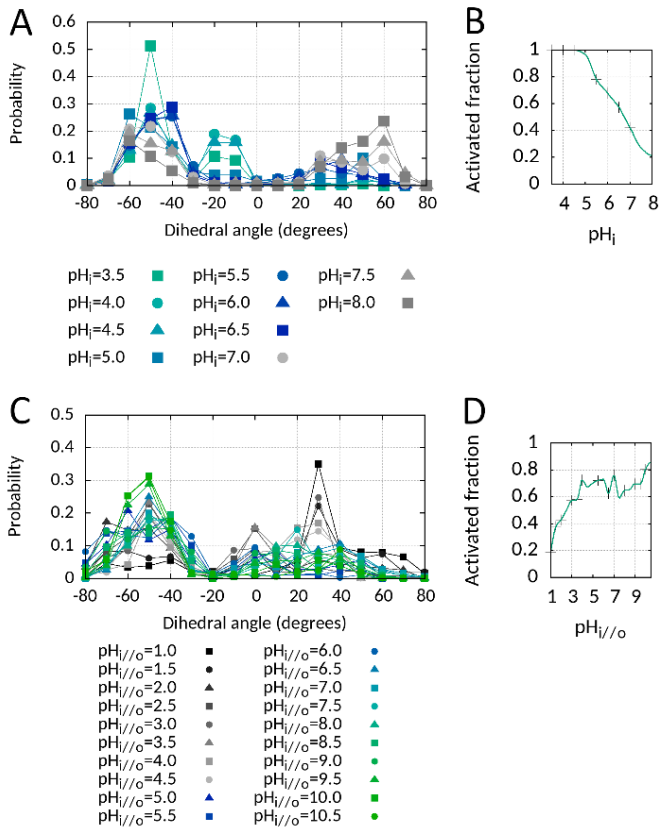

Figure S5. Probability distribution of R208 sidechain (R2sc) dihedral angle with respect to the hydrophobic gasket (HG) in the (A) $\Delta pH_{o=cst}$ and (C) pH_{sym} CpHRE MD simulations**.** The dihedral angle was defined as V177(Cβ)−F150(Cγ)−V109(Cβ)−R208(Cζ). With this definition, R2sc is below the HG at positive dihedral angles and above the HG at negative angles. For the pH_{sym} simulation, only the last 10 ns of the simulation are considered to present more representative results because of the shorter time and lower convergence of the simulation. (B, D) Fraction of activated state based on the dihedral angle for the last 20 ns of the $\Delta pH_{o=cst}$ and last 10 ns of the pH_{sym} CpHRE MD simulations. The pH_{sym} CpHRE MD simulation (C, D) is less converged, also in the last part of the simulation than the $\Delta pH_{i,o=cst}$ simulations, due to the shorter simulated time.

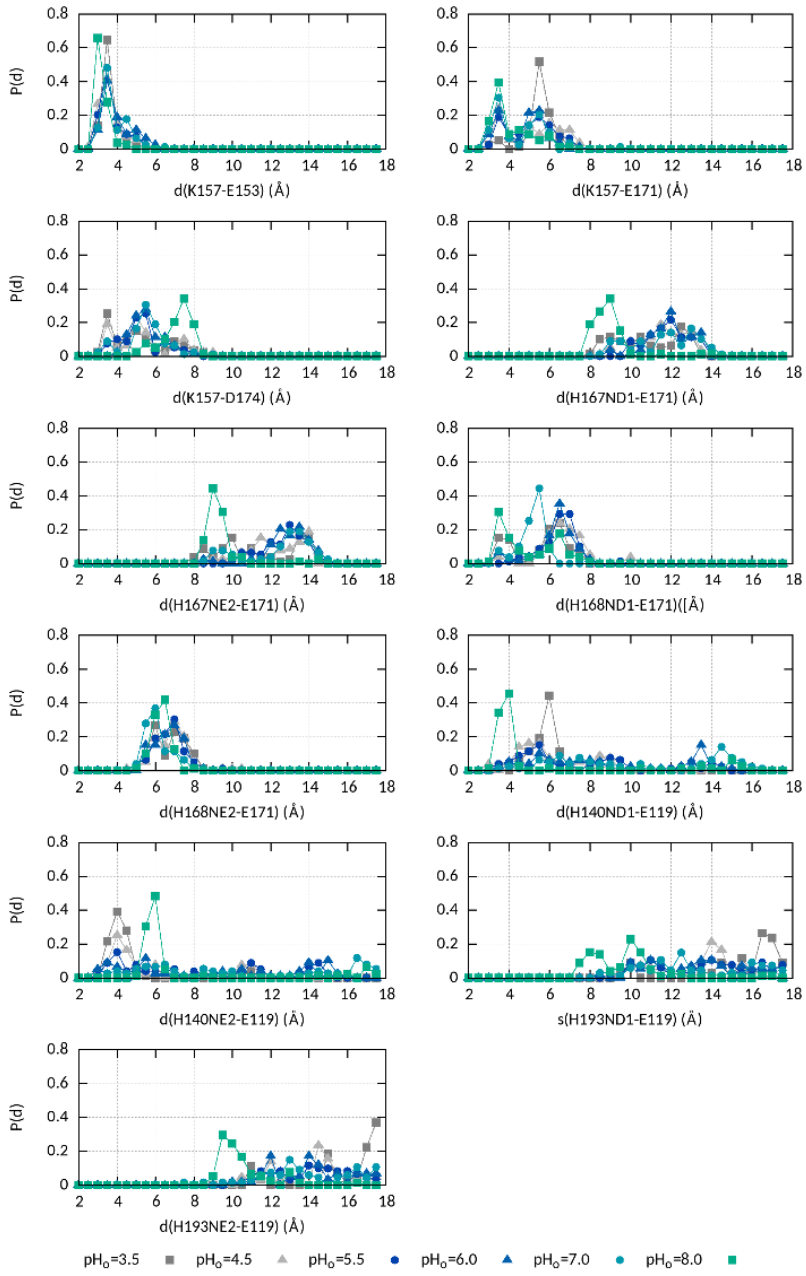

Figure S6. Electrostatic interactions involving amino acids other than the S4 arginines at different pH_o values in the $\Delta pH_{i=cst}$ CpHRE MD simulation. Probability distribution of the distances during the last 20 ns of the simulation at different selected pH_o values.

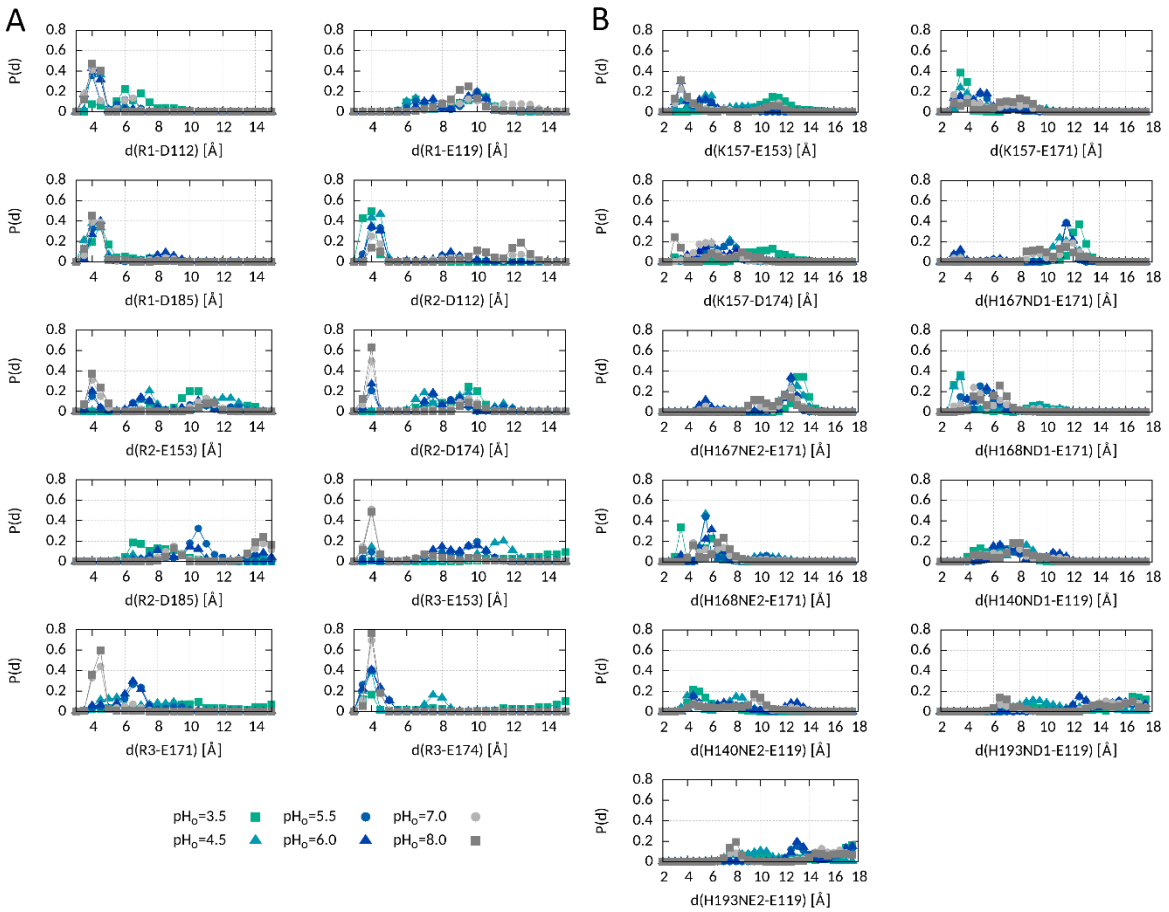

Figure S7. Probability distribution of selected distances in the $\Delta pH_{o=cst}$ (A, B) and pH_{sym} CpHRE MD simulations (C, D). (A) Interactions involving the three S4 Arg R205 (R1), R208 (R2) and R211 (R3) at different pH_i values in the $\Delta pH_{o=cst}$ CpHRE MD simulation. (B) Probability distribution of the distances during the last 20 ns of the simulation at different selected pH_o values.

A

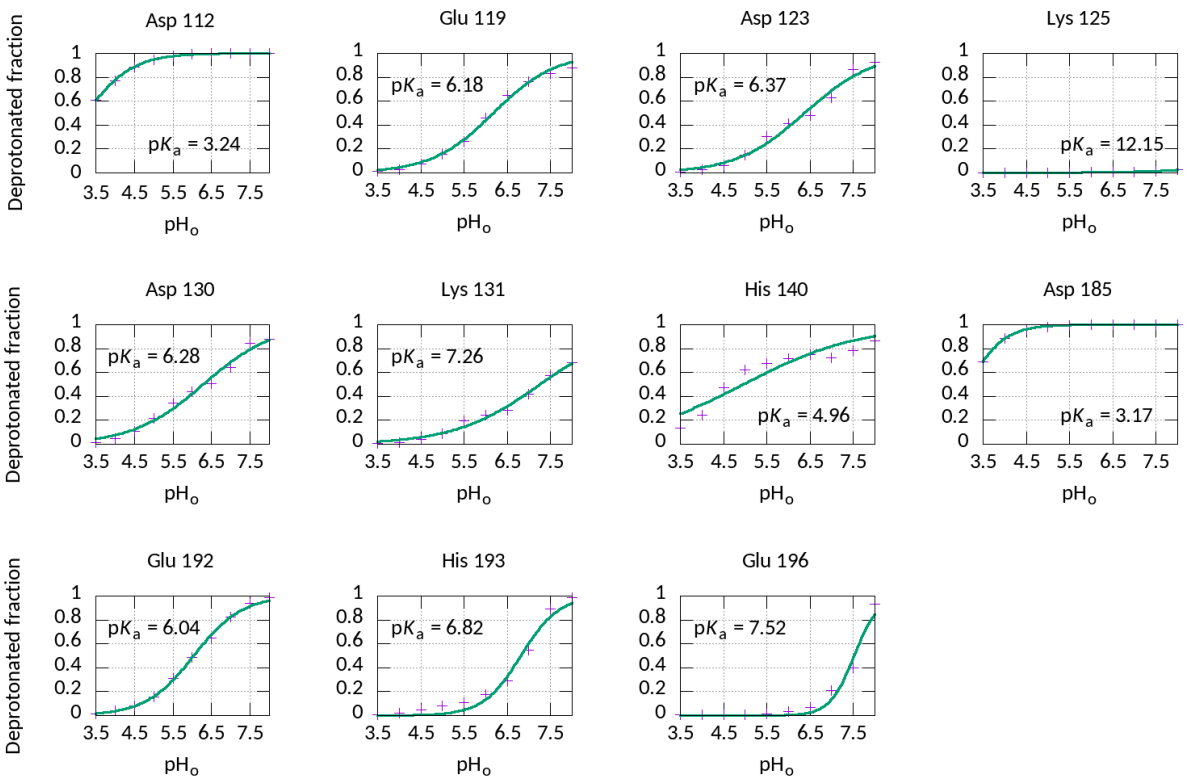
Asp 112
pKa = 3.24
Glu 119
pKa = 6.18
Asp 123
pKa = 6.37
Lys 125
pKa = 12.15
Asp 130
pKa = 6.28
Lys 131
pKa = 7.26
His 140
pKa = 4.96
Asp 185
pKa = 3.17
Glu 192
pKa = 6.04
His 193
pKa = 6.82
Glu 196
pKa = 7.52
Deprotonated fraction
pHo

B

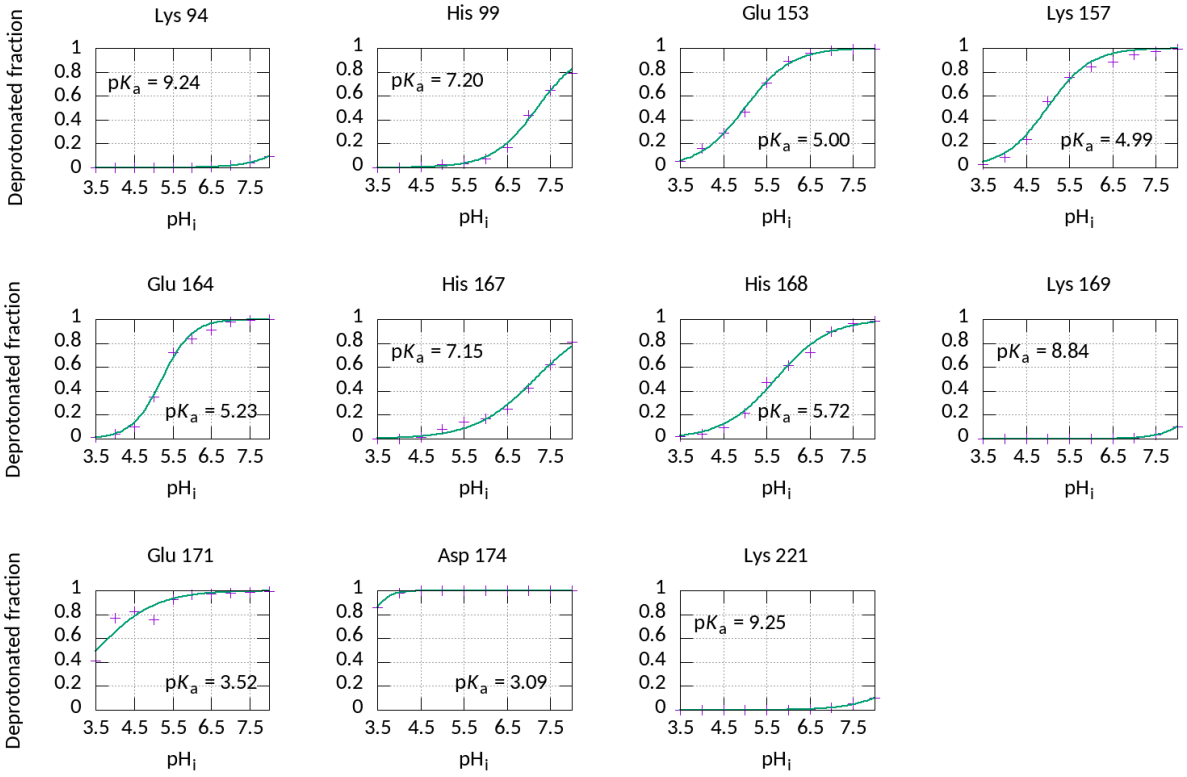
Lys 94
pKa = 9.24
His 99
pKa = 7.20
Glu 153
pKa = 5.00
Lys 157
pKa = 4.99
Glu 164
pKa = 5.23
His 167
pKa = 7.15
His 168
pKa = 5.72
Lys 169
pKa = 8.84
Glu 171
pKa = 3.52
Asp 174
pKa = 3.09
Lys 221
pKa = 9.25
Deprotonated fraction
pHi

C

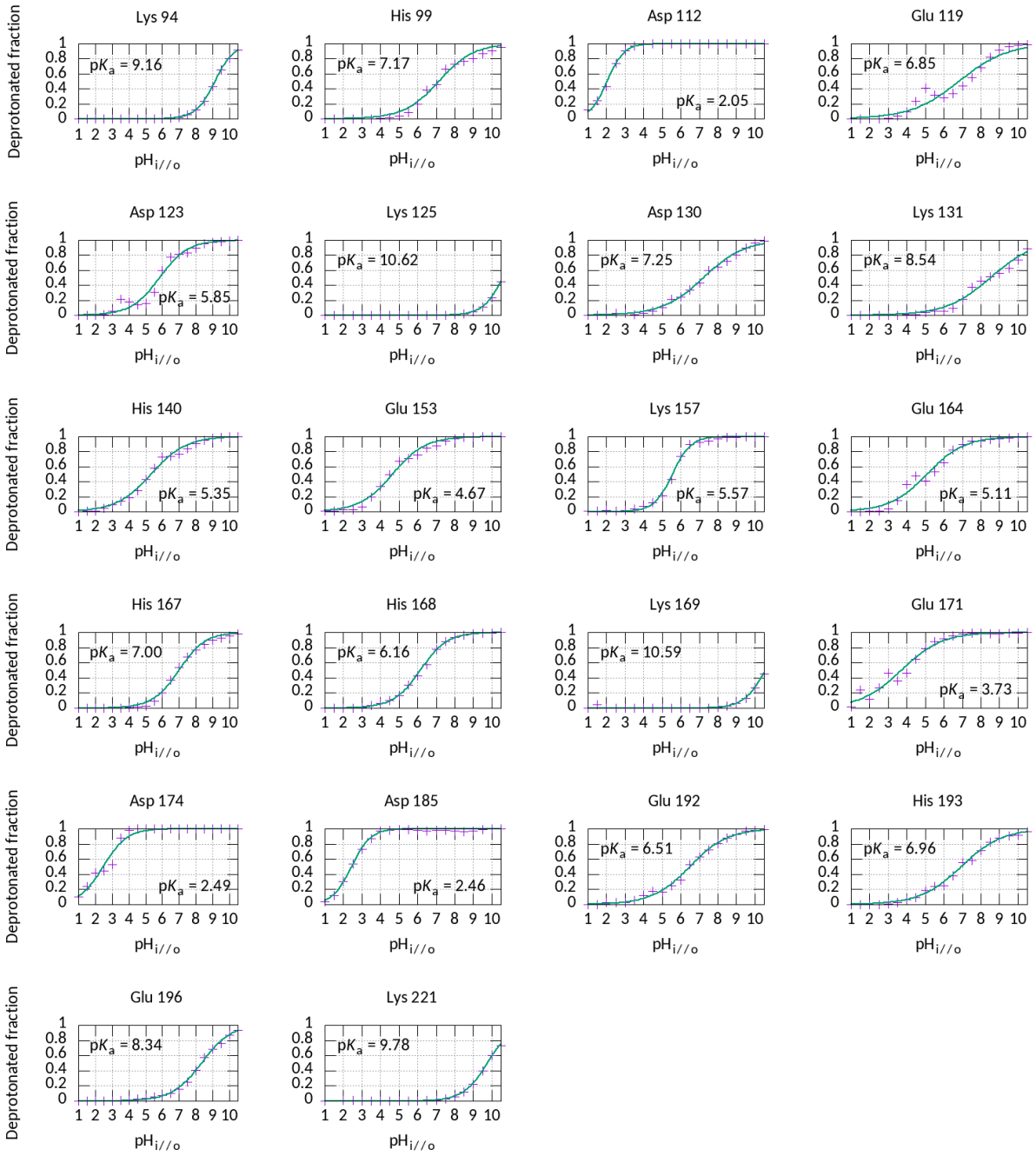

Fig. S8. Titration curves of the individual titratable amino acids sidechains from the (A) $\Delta pH_{i=cst}$, (B) $\Delta pH_{o=cst}$ and (C) ΔpH_{sym} CpHRE MD simulations.